The Healing of Bone Defects by Cell-Free and Stem Cell-Seeded 3D Printed PLA Tissue Engineered Scaffolds

Marjan Bahraminasab (m.bahraminasab@yahoo.com)
Semnan University of Medical Sciences
Athar Talebi
Semnan University of Medical Sciences
Nesa Doostmohammadi
Semnan University of Medical Sciences
Samaneh Arab
Semnan University of Medical Sciences
Ali Ghanbari
Semnan University of Medical Sciences
Sam Zarbakhsh
Semnan University of Medical Sciences

Research Article

Keywords: 3D printing, Bone healing, critical-sized defect, Poly lactic acid, Stem cell

Posted Date: November 30th, 2021

DOI: https://doi.org/10.21203/rs.3.rs-1092132/v1

Abstract

One of the main issues in bone tissue engineering is to realize the response of the host to the engineered scaffolds. In this paper, the in-vivo healing of critical-sized bony defects by cell-free and stem cell-seeded 3D printed PLA scaffolds was studied in rat calvaria bone. First, the scaffolds were 3D printed based on a designed computer model and half of them were seeded by with bone marrow-derived mesenchymal stem cells (BMSCs). The SEM images of the surfaces of PLA and PLA+Cell scaffolds were taken for morphological analysis. All the scaffolds were implanted in the defect sites of rat calvaria bones and histological analysis was conducted after 8 and 12 weeks. The results showed that both cell-free and stem cell-seeded scaffolds exhibited superb healing compared with the empty defect controls. The histological observation revealed the formation of both new bone and connective tissues in the healing site after 8 and 12 weeks, postoperatively. The bone cells including osteoblasts and osteocytes with lacuna were also observed. The higher filled area and the higher bone formation and bone maturation were observed after 12 weeks and in particular for PLA+Cell scaffolds. Furthermore, the systemic toxicity evaluation of the scaffolds using ALT and AST tests reject any toxicity for both cell-free and stem cell-seeded scaffolds. It can be concluded that the 3D printed PLA scaffold with BMSCs seeding has well osteogenic potential to be used for bone defect healing.

1. Introduction

Bony defects in the craniomaxillofacial skeleton due to accidental or surgical trauma are a world wild challenging health concern. Although autologous or allogeneic bone transplantation is a common treatment for bone defects, these have some limitations, such as necrosis, infection, pain, and risk of morbidity, therefore, other alternative methods are needed (Szpalski et al. 2010, Azi et al. 2016). Tissue engineering and regenerative medicine try to use a combination of bioactive materials, growth factors, and cell therapy to repair bone tissue (Bahraminasab 2020, Zhang et al. 2020). Due to the osteogenic effect, treatment with cells, especially mesenchymal stem cells (MSCs) may be advantageous in treating critical bone defects caused by severe trauma, osteoporosis, aging, and metabolic diseases like diabetes. The recruitment and migration of MSCs from neighboring tissues to the injured area or defect might not be adequate for differentiation into osteogenic precursor cells in severe bone defects (Watanabe et al. 2016). Therefore, MSCs can be applied more effectively embedded/seeded in/on the scaffold to differentiate into osteo-progenitor cells at the defect site. It has been shown that the seeded MSCs on the scaffold can migrate to the defect site, recruit the source of precursor cells, and finally increase the rate of the scaffold degradation under in vivo conditions. The appropriate biodegradable scaffold assists the migration, adhesion, and proliferation process of stem cells (Diomede et al. 2018, Han et al. 2020, Liu et al. 2020, Oryan et al. 2020).

Choosing the suitable material is very important for the manufacture of scaffolds in bone generation, in this aspect three basic characteristics of biomaterials which include bioactivity, biocompatibility, and biodegradability must be considered in each assay (Ho-Shui-Ling et al. 2018). Poly lactic acid (PLA) is a popular biodegradable polymer with a broad range of applications including medical implant devices,

and scaffolds in tissue engineering. The broad use of PLA is due to a combination of favorable properties including its unique biocompatibility, acceptable bioresorbability, generation of nontoxic byproducts during the degradation in the body, and approved clinical trials by the US Food and Drug Administration (FDA) (Persson et al. 2014). Furthermore, PLA can be easily printed into scaffolds with different architectures/internal structures and external shapes (Gregor et al. 2017, Wurm et al. 2017, Buj-Corral et al. 2018, Corcione et al. 2019). Therefore, in the current study, PLA was chosen to serve as a template for the delivery of MSCs to the defect site in the rat calvaria. For comparison, the PLA cell-free scaffolds were also implanted and the results were compared. To the authors' knowledge, there is no study on evaluation of the 3D printed PLA scaffold along with MSCs in an in-vivo study.

2. Materials And Methods

2.1. 3D printing of PLA scaffolds

First, a 3D computer-aided design (CAD) model of the PLA scaffold was designed in ABAQUS software. Subsequently, the "stl." File format of the model was imported to Simplify3D software to provide the g-codes for manufacturing. Poly(lactic) acid filament (diameter of 1.75 mm) was used to build the scaffolds with a conventional fused deposition modeling (FDM) printer. The PLA filament was heated above the PLA melting temperature (nozzle temperature was 210ºC). The melted PLA was extruded through a nozzle made up of stainless-steel on to a printing bed having temperature of 60ºC. The scaffolds were printed in a layer-by-layer manner having a 7.6 mm diameter and a 1.6 mm height. The strut thickness was 0.4 mm and the pore size was 800 µm. The fabricated PLA scaffolds were analyzed using X-ray diffraction (XRD) technique (Bruker, D8-advance) and Attenuated Total Reflection-Furrier Transform Infrared Spectroscopy (ATR-FTIR, Bruker's Alpha FTIR Spectrometer, Germany). The XRD analysis was conducted at 35 kV and 30 mA using Cu Kα radiation (λ=1.5405980 Å). The scanning angle (2θ) was between 5°-80° at a step size of 0.06°. ATR-FTIR spectrum was obtained at the resolution of 2 cm^{-1} over the frequency range of 4000-600 cm^{-1}.

2.2. BMSCs harvesting, culture and immunophenotype

The BMSCs harvesting and culture were done based on the previous study (Talebi et al. 2020). Briefly, after sacrificing an adult female rat, the femur and tibia were immediately removed. To kill the rat, it was first anesthetized by intraperitoneal injection of 80 mg/kg ketamine and 10 mg/kg xylazine, and it was followed by cervical dislocation. The bone marrow was flushed by 10 ml of Dulbecco's Modified Eagle Medium (DMEM, Gibco) with nutrient F12 Ham, supplemented with 10% fetal bovine serum (FBS, Gibco) in two T25 tissue culture flasks, and incubated in the culture medium containing 10% FBS and 1% penicillin/streptomycin at 37 °C, 95% humidity, and 5% CO_2. After 48 hours, the culture medium was replaced. Adhesive cells were sub-cultured four times upon reaching 80–90% confluence.

To analyze the expression of BMSCs surface markers, more than 1×10^5 cells were incubated in fluorescently labeled monoclonal antibodies (BD Pharmingen) against CD29, CD34, CD44, CD45 and

CD90 in a dark place. After 30 minutes of washing with PBS, the labeled cells were analyzed using flow cytometry (BD FACS Calibur). Furthermore, optical microscopy images were taken at different passages for morphology evaluation.

2.3. Sterilizing the PLA scaffolds

The 3D printed PLA scaffolds were first immersed in distilled water for 1 h. Then, they were washed and ultrasonically cleaned with distilled water for 5 minutes. Afterward, the cleaned samples were sterilized using ultra-violet (UV) light under a laminar flow bench; 10 min each side of the scaffolds. For the cell-free group, each sterilized PLA scaffold was individually put in a sterile petri dish and transferred for surgery. For the cell-seeded group, the sterilized PLA scaffolds were used to seed MSCs. After seeding (as explained in the following section), each cell-seeded scaffold was individually put in a sterile petri dish with a small amount of complete medium (500µL) and transferred for implantation.

2.4. BMSCs seeding and culturing on PLA scaffolds

Initially, the bottom of wells of a 24-well plate was evenly coated by 2% agarose (700 µL per well) having no defects including bubbles or scratches in the coatings. After ≈30 minutes, the sterilized PLA scaffolds were placed on the agarose. For seeding, 230 µL of culture medium containing 10^6 BMSCs was added evenly on both sides of the scaffolds; 115 µL on each side. After seeding of the cells on each side of the scaffold, a time interval of about 20 minutes was considered for initial cell attachment. In the next step, 1 mL of additional culture medium was gently added to each well and the plate was placed in an incubator at 37 °C, with 95% humidity and 5% CO_2 for 24h. Finally, the seeded scaffolds were transferred for surgery one-by-one.

2.5. Animals

Wistar female (n=24) adult rats, weighing 250 ± 20 g were used in this study. Animals were kept in a controlled temperature (22 ± 2°C) place and a 12-h regular light/dark cycle (light on from 07:00 to 19:00), housed 2 to 4 per cage with free access to food and water (Safakhah et al. 2017). The experimental protocol was approved by the Ethical Review Board of Semnan University of Medical Sciences (Ethic code: IR.SEMUMS.REC.1400.048). All experiments were conducted in agreement with the National Institutes of Health Guide for the Care and Use of Laboratory Animals.

2.6. Implantation

The scaffold implantation was performed through a method which was described by Sadeghi et al. (Sadeghi et al. 2016). After anesthetizing of the rats by intraperitoneal (IP) injection of a mixture containing ketamine hydrochloride and xylazine hydrochloride with the volume ratio of 8:2 at 1mL/kg (Bahraminasab et al. 2021), the head of the rat was completely fixed in a stereotaxic apparatus, and the hair was shaved and the skull was disinfected using povidone iodine solution. To expose the full extent of the calvaria, subperiosteal dissection was done bilaterally in a non-infectious manner and the

subcutaneous muscles were completely pushed away. The skull was drilled to the size of the scaffold using a surgical trephine bur. One calvaria through-and-through osteotomy was made in the dorsal portion of the parietal bone midsagittal suture (Figure 1a) under irrigation with sterile normal saline. After preparing the transplant conditions, the scaffold was placed into the whole and finally, the scalp was sutured. The bone repair was analyzed after 8 and 12 weeks, postoperatively. The details of animal groups are given in Table 1.

Table 1: Details of studied animal groups

Group number	Group name	Time (week)	Number of implanted rats for each implantation time
1	defect	8	2
		12	2
2	PLA	8	5
		12	5
3	PLA+Cell	8	5
		12	5

2.7. Histological analysis

The histological analysis was conducted after 8 and 12 weeks. First, the rats were sacrificed and then the defect sites were judiciously dissected. These samples were fixed in neutral-buffered formalin (10%), and decalcified in formic acid (10%), sequentially. The standard dehydration was then conducted on the decalcified samples in serially increasing alcohol (ethanol) solutions. The dehydrated samples were embedded in paraffin and subsequently 5μm sections were provided. The prepared sections were stained with hematoxylin and eosin (H&E). The analyzed area in histology is shown in Figure 1b. Some sections were also stained by toluidine blue. A light microscope was employed to analyze the histology slides. The percentages of the new bone area were measured from H&E images using ImageJ software. Furthermore, immediately after harvesting the defect sites, photos were taken and the macroscopically filled area by new bone was calculated in percent using ImageJ software. Figure 2, shows the whole procedure used in this study.

2.8. Serum biochemistry and osteocalcin detection

To assess the systemic toxicity of the scaffolds, the level of liver and muscle enzymes was measured by serum biochemistry. At the time of sacrifice (8 or 12 weeks postoperatively), about 5 mL of blood was collected from the heart of each rat and centrifuged at 3000 rpm for 10 min to obtain blood serum. Alanine aminotransferase (ALT) and aspartate aminotransferase (AST) were analyzed using the commercial kits (Paadco, Golestan Technology Park, Iran). Furthermore, the osteocalcin level (a bone formation marker) was also measured in the serum, using a sandwich ELISA method (Rat

Osteocalcin/Bone Gamma-Carboxyglutamic Acid Containing Protein (OT/BGLAP) EISA Kit; ZellBio, Germany) according to the manufacturer instruction.

2.9. Statistical analysis

Analysis of Variance (ANOVA) was done for statistical analyses using Minitab V17 software. The confidence level was set to be 95% (α=0.05) in all analyses. Moreover, the post-hoc pairwise comparisons were conducted using Tukey test.

3. Results

3.1. Phase analysis and chemical bonds

Figure 3a shows a noisy background with no sharp and narrow diffraction peaks in PLA indicating its amorphous nature. There is a large broad peak extending from 2θ of around 10◦ to <30◦. Two small peaks also can be seen at 5◦<2θ<10◦ and 30◦<2θ<35◦. The obtained pattern corresponds to the characteristic peak of PLA (Zhang et al. 2011, Burgos et al. 2013, Armentano et al. 2015, Lu et al. 2016). The ATR-FTIR spectra of PLA scaffold is shown in Figure 3b. The characteristic bands at about 2994 cm^{-1} and 2944 cm^{-1} are related to –CH stretching in $–CH_3$ group. The peak appeared at 2922 cm^{-1} is attributed to –CH bending vibration. Furthermore, some peaks were also observed at 756 and 867 cm^{-1} (–CH bending vibration); 1043 cm^{-1} and 1182 cm^{-1} (C–O stretching vibration); 1082 cm^{-1} (stretching peaks of C–O–C bonds) 1451 cm^{-1} and 1361 cm^{-1} (–CH bending in –CH3 group); and 1748 cm^{-1} (C=O stretching vibration on ester group). The observed peaks correspond to PLA and agree well with data in the previous studies (Yang et al. 2008, Revati et al. 2017, Ozaltin et al. 2020).

3.2. BMSCs morphology and immunophenotype

The morphology of the BMSCs was observed during culturing which was appeared to be normal; adherent in spindle shape with fibroblastic morphology (Chen et al. 2014, Wang et al. 2017). Figure 4 shows the morphology of BMSCs during culture (passages 1 and 3). The flow cytometry analysis was illustrated that BMSCs isolated from rat bone marrow were positive for the cell surface markers CD29 (94.92%), CD44 (93.68%), and CD90 (95.84%), while were negative for CD34 (6.26%) and CD45 (4.40%) (Figure 5). These results suggested that the cultured cells have similar morphological and immunophenotypical characteristics to BMSCs.

3.3. Seeded BMSCs on scaffolds

Immediately, after cell seeding (live cells) as well as after fixation, the PLA scaffolds were observed under an optical microscope. As it can be seen in Figure 6, a dense cell layer was seeded on the scaffolds. Furthermore, SEM images were taken from the surface and cross- section of a PLA scaffold (Figures 7a and 7b), and from the surface of the scaffold with fixed cells (Figures 7c-7f). In these figures, the scaffold is shown by "S" and the cell layer is indicated by "C".

3.4. Histology and histomorphometry analysis

Figures 8 and 9 show the histological H&E images taken 8 and 12 weeks after implantation, respectively. In these figures, the scaffold is shown by the letter "S" (light beige color), the defect is identified by the letter "D", and the bone is marked by the letter "B" (pink color). The osteocytes are indicated in rectangles and the new bone islands are pointed at by arrows. The scaffolds still remained at the defect site meaning that the biodegradability of the PLA scaffold was slow. However, the new tissues including connective, and neo-bone were formed around the scaffold struts in the pores. In the PLA groups more connective tissues and collagen fibers, and smaller bone, particularly in the lamellar form were observed. However, these were more obvious at week 8 rather than week 12. In the PLA+Cell groups, more blood vessel formation and a small number of lymphocytes (yellow circle in Figure 8) were observed. A higher degree of new bone formation, more lamellar bone and cartilaginous tissue were observed in the PLA+Cell groups compared with cell-free PLA scaffolds. As it can be seen in Figures 8a and 9a, minimum tissue formation was seen in the untreated defect group.

Figure 10a shows the percentages of the bone area formed in the defect site around the scaffolds. The mean values of bone area% for PLA and PLA+Cell were 30.0% and 41.2%, and 53.5% and 59.8% after 8 and 12 weeks, respectively. In addition, a higher new bone area was observed in the defect sites after 12 weeks in both groups. The ANOVA results revealed that implantation time was a significant factor on bone area formed (P-value=0.000). Nevertheless, the scaffold type was not significant (P-value=0.081), at the confidence level of 95%. In Figure 10, the means that do not share a letter are significantly different (results of Tukey test). Therefore, the new bone area formed around PLA scaffolds after 8 weeks was significantly lower than PLA and PLA+Cell scaffolds after 12 weeks. Meanwhile, the bone area% in the defect site around PLA+Cell scaffolds after 8 weeks was significantly different from that after 12 weeks. However, there were no statistically significant differences between PLA and PLA+Cell scaffolds after 8 weeks as well as after 12 weeks. Figure 10b represents the filled area of the defect by new tissue in the studied groups. The values in this figure were normalized to the defect size at the operation day. As it can be seen the filled area increased in all groups at week 12 compared to week 8. Furthermore, the filled area was highest for the PLA+Cell group 12 weeks, postoperatively. The results of ANOVA also indicated that the scaffold is a significant factor in filled area% (P value=0.000). The Tukey pairwise comparisons indicated that the areas of the defect filled by new tissue (both soft and hard tissues) were significantly higher in PLA and PLA+Cell group compared with the untreated control group (defect without scaffold). It should be pointed out that in the untreated group the filled area of the defects was mostly non-functional soft tissue, while in the scaffold groups, as indicated by H&E staining, the filled area mainly had cartilaginous and bone tissues.

Toluidine blue, a cationic dye, stains the proteoglycans as well as glycosaminoglycans in the tissue (Schmitz et al. 2010). Proteoglycans are one of the most abundant constituents of the non-collagenous proteins in the bone matrix. These are characterized by the covalent bond of long-chain polysaccharides (glycosaminoglycans) to core protein molecules (Robey 2002). Therefore, toluidine blue stains the tissue where bone matrix and connective tissue are formed. Figures 11 and 12 show the toluidine blue staining

of the tissues 8 and 12 weeks after implantation. As it can be seen in these figures, in the PLA+Cell groups both new bone and connective tissue were clearly observed. These features were also seen in the PLA group at week 12. However, at week 8, the area of the colored tissue was very small as shown in Figures 11a and 11b.

3.5. ALT, AST, and osteocalcin level

The biochemical analyses (ALT and AST level) were performed to monitor the systemic influence and any abnormal response possibly induced by the scaffolds. AST and ALT are sensibly sensitive indicators of liver injury or damage from various types of diseases or conditions. The ALT and AST levels in rat serum of different groups are shown in Figure 13. The continuous red line and dashed blue line in Figure 13 indicate these enzyme levels for normal female rats with neither skull defects nor scaffold implantation. The AST levels in all groups of scaffolds did not exceed the dashed blue line meaning that the scaffolds did not cause systemic toxic effects. Similarly, the ALT levels did not surpass the normal level except for the rats with PLA scaffold implantation after 8 weeks. However, after 12 weeks the ALT value decreased below the reference line. Furthermore, there were no significant differences between groups in ALT and AST levels.

The serum osteocalcin levels (Table 2) were higher at week 8 than week 12 in all groups. The highest osteocalcin level was associated with PLA+Cell at week 8. The level of this osteoblastic marker was lower at week 12 possibly due to the fact that after this time the defects were mostly filled by new bone. The level of osteocalcin in the PLA+Cell group at week 12 was significantly different PLA+Cell and PLA at week 8, and PLA at week 12. Nevertheless, the level of osteocalcin in the defect group was not change at weeks 8 and 12. This is due to the fact that no bone matrix was formed at the defect site in this group.

Table 2: Osteocalcin levels in rat serum of studied groups

group	Time (weeks)	Osteocalcin (ng/mL)
defect	8	2.196±0.147
	12	2.136±0.059
PLA	8	2.092±0.056
	12	2.031±0.022
PLA+Cell	8	2.417±0.084
	12	1.792±0.050

4. Discussion

In present paper, the efficacy of 3D printed PLA scaffolds both as cell-free and cell-seeded construct was assessed in the repair of a critical-sized defect in rat calvaria. Our findings suggest that both scaffolds provide efficient templates for new bone growth and repair without producing any toxic effects. The ALT and AST levels in blood serum are indicative of the systemic influence of the implanted scaffolds on liver function (Masuzaki et al. 2010, Lai et al. 2019, Shuai et al. 2020). In the results obtained here, the levels of these two enzymes laid below the normal levels. PLA is a synthetic polymer that is widely used in tissue engineering applications and its high biocompatibility has been reported frequently (Llorens et al. 2015, Da Silva et al. 2018, Mazur et al. 2020, Zimina et al. 2020). Our findings also rejected any toxicity or abnormality caused by neither scaffold material nor the manufacturing approach.

The osteocalcin concentration was measured in blood serum. Osteocalcin is produced only by mature osteoblasts and plays a role in bone mineralization (Ayukawa et al. 2010). It is mainly deposited into the bone extra cellular matrix (ECM) and only a small quantity of its newly formed reaches the circulation (Zhang et al. 2004, Tarafder et al. 2013). The highest osteocalcin level in PLA+Cell at week 8 might indicate the higher mineralization in this group (as confirmed by the result shown in Figure 10a). The level of this osteoblastic marker at week 12 was lower in all groups and it may be due to the fact that after this time the defects were mostly filled by new bone. In one study conducted by Zhang and Zhang (Zhang et al. 2004), the osteocalcin expression by MG63 exposed to microporous chitosan scaffolds reinforced by calcium phosphate was assessed. The authors obtained lower osteocalcin concentration at day 11 compared with that of day 7. Their result on reduction of osteocalcin level by time in in agreement with our findings. Another point is that the level of this osteoblastic marker in the defect group was not change at different time points. This is due to the fact that no bone matrix was formed at the defect site in this group.

Both PLA and PLA+Cell scaffolds showed to induce tissue regeneration at the defect site. The connective and bone tissues along with collagen fibers and blood vessels were formed around the scaffold struts. However, the histological analysis revealed that the PLA+Cell scaffolds caused better bone formation and repair. The presence of BMSCs on the scaffold appeared to help in the bone regeneration process. MSCs are known as self-renewing, multipotent cells, which exist in different body tissues and are considered as reparative cell reservoirs. These cells differentiate in response to signaling at the site of injury (Gordon et al. 2006, Marei et al. 2016). Furthermore, MSCs can contribute to the maintenance of stem cell niche and tissue homeostasis (Hsu et al. 2012). Moreover, they have low immunogenicity and show effective immune-suppressive qualities. Nevertheless, the MSCs recruitment and migration from adjacent tissues to the defect site is not probably adequate for differentiation into osteogenic precursor cells in severe bone defects (Watanabe et al. 2016), such as the critical-sized defect (7.6 mm) in the present study. Therefore, scaffolds can be employed to have a more effective migration of the MSCs differentiating into osteo-progenitor cells at the defect area. The promising results of our histological analysis suggest that the PLA scaffold provided an appropriate environment for the viability of the BMSCs. This can be attributed to the scaffold structural characteristics including proper biomaterial composition, porosity percentage, and pore sizes (Qazi et al. 2019, Teixeira et al. 2019, Oryan et al. 2020, Tytgat et al. 2020). These properties along with mechanical stability, stiffness, biodegradation, and non-toxicity are required

for the successful performance of an implanted scaffold (Bahraminasab et al. 2018, Bahraminasab et al. 2019). PLA has this combination of properties which results in an acceptable function in-vivo. The only drawback of PLA is its hydrophobicity and reduced cell adhesion (Armentano et al. 2010). Therefore, some studies focused on PLA modification using bioceramics or surface treatments (Wang et al. 2016, Tatullo et al. 2019). It would be interesting to study the in-vivo performance of the treated PLA and its composites along with BMSCs to find out about the synergistic and antagonistic effects. Another issue that can be considered in future studies is the used of growth factors that can provide the proper signaling and help in stem cell differentiation (Tollemar et al. 2016).

5. Conclusions

The results from this study showed the two scaffolds can encourage effective healing of a critical-sized defect in rat calvaria compared to the untreated controls (empty defects without scaffolds). The 3D printed porous PLA scaffold was a suitable framework for BMSCs seeding as they could differentiate to bone cells and contribute to the healing. According to the results obtained here, the osteogenesis of the 3D printed PLA scaffold were enhanced after loading it with the BMSCs. Therefore, the scaffold has the potential for future bone tissue engineering applications.

Abbreviations

3D: three dimensional

ALT: alanine aminotransferase

ANOVA: analysis of variance

AST: aspartate aminotransferase

ATR-FTIR: Attenuated Total Reflection-Furrier Transform Infrared Spectroscopy

BMSCs: bone marrow-derived mesenchymal stem cells

CAD: computer-aided design

DMEM: Dulbecco's Modified Eagle Medium

ECM: extra cellular matrix

FDA: food and drug administration

FDM: fused deposition modeling

H&E: hematoxylin and eosin

IP: intraperitoneal

MSCs: mesenchymal stem cells

PLA: poly lactic acid

SEM: scanning electron microscopy

UV: ultra violet

XRD: X-ray diffraction

Declarations

Ethics approval and consent to participate

The animal experimental protocol was approved by the Ethical Review Board of Semnan University of Medical Sciences (Ethic code: IR.SEMUMS.REC.1400.048).

Consent for publication

Not Applicable

Availability of data and material

The data will be available upon request.

Competing interests

The authors declare that they have no conflict of interest.

Funding

This study was funded by Semnan University of Medical Sciences (NO. 1876).

Authors' contributions

Marjan Bahraminasab: conceptualization, data analysis, provision of study materials. experimentation, draft preparation, and writing and reviewing

Athar Talebi: experimentation

Nesa Doostmohammadi: experimentation

Samaneh Arab: experimentation, reviewing and editing

Ali Ghanbari: experimentation**,** reviewing and editing

Sam Zarbakhsh: experimentation, reviewing and editing

Acknowledgements

The authors would like to thank Semnan University of Medical Sciences for funding this work (NO. 1876).

6. References

1. Armentano, I., M. Dottori, E. Fortunati, S. Mattioli and J. Kenny (2010). Biodegradable polymer matrix nanocomposites for tissue engineering: a review. Polymer degradation and stability **95**(11): 2126-2146.
2. Armentano, I., E. Fortunati, N. Burgos, F. Dominici, F. Luzi, S. Fiori, A. Jiménez, K. Yoon, J. Ahn and S. Kang (2015). Processing and characterization of plasticized PLA/PHB blends for biodegradable multiphase systems.
3. Ayukawa, Y., Y. Ogino, Y. Moriyama, I. Atsuta, Y. Jinno, M. Kihara, Y. Tsukiyama and K. Koyano (2010). Simvastatin enhances bone formation around titanium implants in rat tibiae. Journal of oral rehabilitation **37**(2): 123-130.
4. Azi, M. L., A. Aprato, I. Santi, M. Kfuri, A. Masse and A. Joeris (2016). Autologous bone graft in the treatment of post-traumatic bone defects: a systematic review and meta-analysis. BMC musculoskeletal disorders **17**(1): 1-10.
5. Bahraminasab, M. (2020). Challenges on optimization of 3D-printed bone scaffolds. BioMedical Engineering OnLine **19**(1): 1-33.
6. Bahraminasab, M., S. Arab, M. Safari, A. Talebi, F. Kavakebian and N. Doostmohammadi (2021). In vivo performance of Al 2 O 3-Ti bone implants in the rat femur. Journal of Orthopaedic Surgery and Research **16**(1): 1-14.
7. Bahraminasab, M. and K. L. Edwards (2018). Biocomposites for Hard Tissue Replacement and Repair. Futuristic Composites. Materials Horizons: From Nature to Nanomaterials,. B. P. Sidhu S., Zitoune R., Yazdani M. (Eds). Singapore, Springer**:** 281-296.
8. Bahraminasab, M. and K. L. Edwards (2019). Computational Tailoring of Orthopaedic Biomaterials: Design Principles and Aiding Tools. Biomaterials in Orthopaedics and Bone Regeneration, Springer**:** 15-31.
9. Buj-Corral, I., A. Bagheri and O. Petit-Rojo (2018). 3D printing of porous scaffolds with controlled porosity and pore size values. Materials **11**(9): 1532.
10. Burgos, N., V. P. Martino and A. Jiménez (2013). Characterization and ageing study of poly (lactic acid) films plasticized with oligomeric lactic acid. Polymer degradation and stability **98**(2): 651-658.
11. Chen, Q., Y. Yuan and T. Chen (2014). Morphology, differentiation and adhesion molecule expression changes of bone marrow mesenchymal stem cells from acute myeloid leukemia patients. Molecular medicine reports **9**(1): 293-298.

12. Corcione, C. E., F. Gervaso, F. Scalera, S. K. Padmanabhan, M. Madaghiele, F. Montagna, A. Sannino, A. Licciulli and A. Maffezzoli (2019). Highly loaded hydroxyapatite microsphere/PLA porous scaffolds obtained by fused deposition modelling. Ceramics International **45**(2): 2803-2810.
13. Da Silva, D., M. Kaduri, M. Poley, O. Adir, N. Krinsky, J. Shainsky-Roitman and A. Schroeder (2018). Biocompatibility, biodegradation and excretion of polylactic acid (PLA) in medical implants and theranostic systems. Chemical Engineering Journal **340**: 9-14.
14. Diomede, F., A. Gugliandolo, P. Cardelli, I. Merciaro, V. Ettorre, T. Traini, R. Bedini, D. Scionti, A. Bramanti and A. Nanci (2018). Three-dimensional printed PLA scaffold and human gingival stem cell-derived extracellular vesicles: a new tool for bone defect repair. Stem cell research & therapy **9**(1): 104.
15. Gordon, M. Y., N. Levičar, M. Pai, P. Bachellier, I. Dimarakis, F. Al-Allaf, H. M'Hamdi, T. Thalji, J. P. Welsh and S. B. Marley (2006). Characterization and clinical application of human CD34+ stem/progenitor cell populations mobilized into the blood by granulocyte colony-stimulating factor. Stem cells **24**(7): 1822-1830.
16. Gregor, A., E. Filová, M. Novák, J. Kronek, H. Chlup, M. Buzgo, V. Blahnová, V. Lukášová, M. Bartoš and A. Nečas (2017). Designing of PLA scaffolds for bone tissue replacement fabricated by ordinary commercial 3D printer. Journal of biological engineering **11**(1): 31.
17. Han, S. H., M. Cha, Y.-Z. Jin, K.-M. Lee and J. H. Lee (2020). BMP-2 and hMSC dual delivery onto 3D printed PLA-Biogel scaffold for critical-size bone defect regeneration in rabbit tibia. Biomedical Materials **16**(1): 015019.
18. Ho-Shui-Ling, A., J. Bolander, L. E. Rustom, A. W. Johnson, F. P. Luyten and C. Picart (2018). Bone regeneration strategies: Engineered scaffolds, bioactive molecules and stem cells current stage and future perspectives. Biomaterials **180**: 143-162.
19. Hsu, Y.-C. and E. Fuchs (2012). A family business: stem cell progeny join the niche to regulate homeostasis. Nature reviews Molecular cell biology **13**(2): 103-114.
20. Lai, Y., Y. Li, H. Cao, J. Long, X. Wang, L. Li, C. Li, Q. Jia, B. Teng and T. Tang (2019). Osteogenic magnesium incorporated into PLGA/TCP porous scaffold by 3D printing for repairing challenging bone defect. Biomaterials **197**: 207-219.
21. Liu, Z., Y. Ge, L. Zhang, Y. Wang, C. Guo, K. Feng, S. Yang, Z. Zhai, Y. Chi and J. Zhao (2020). The effect of induced membranes combined with enhanced bone marrow and 3D PLA-HA on repairing long bone defects in vivo. Journal of Tissue Engineering and Regenerative Medicine **14**(10): 1403-1414.
22. Llorens, E., S. Calderón, L. J. del Valle and J. Puiggalí (2015). Polybiguanide (PHMB) loaded in PLA scaffolds displaying high hydrophobic, biocompatibility and antibacterial properties. Materials Science and Engineering: C **50**: 74-84.
23. Lu, F., H. Yu, C. Yan and J. Yao (2016). Polylactic acid nanocomposite films with spherical nanocelluloses as efficient nucleation agents: effects on crystallization, mechanical and thermal properties. RSC advances **6**(51): 46008-46018.

24. Marei, N. H., I. M. El-Sherbiny, A. Lotfy, A. El-Badawy and N. El-Badri (2016). Mesenchymal stem cells growth and proliferation enhancement using PLA vs PCL based nanofibrous scaffolds. International journal of biological macromolecules **93**: 9-19.
25. Masuzaki, T., Y. Ayukawa, Y. Moriyama, Y. Jinno, I. Atsuta, Y. Ogino and K. Koyano (2010). The effect of a single remote injection of statin-impregnated poly (lactic-co-glycolic acid) microspheres on osteogenesis around titanium implants in rat tibia. Biomaterials **31**(12): 3327-3334.
26. Mazur, K., R. Singh, R. P. Friedrich, H. Genç, H. Unterweger, K. Sałasińska, R. Bogucki, S. Kuciel and I. Cicha (2020). The effect of antibacterial particle incorporation on the mechanical properties, biodegradability, and biocompatibility of PLA and PHBV composites. Macromolecular Materials and Engineering **305**(9): 2000244.
27. Oryan, A., S. Hassanajili, S. Sahvieh and N. Azarpira (2020). Effectiveness of mesenchymal stem cell-seeded onto the 3D polylactic acid/polycaprolactone/hydroxyapatite scaffold on the radius bone defect in rat. Life Sciences **257**: 118038.
28. Ozaltin, K., E. Vargun, A. Di Martino, Z. Capakova, M. Lehocky, P. Humpolicek, N. Kazantseva and P. Saha (2020). Cell response to PLA scaffolds functionalized with various seaweed polysaccharides. International Journal of Polymeric Materials and Polymeric Biomaterials: 1-8.
29. Persson, M., G. S. Lorite, H. E. Kokkonen, S.-W. Cho, P. P. Lehenkari, M. Skrifvars and J. Tuukkanen (2014). Effect of bioactive extruded PLA/HA composite films on focal adhesion formation of preosteoblastic cells. Colloids and Surfaces B: Biointerfaces **121**: 409-416.
30. Qazi, T. H., L. Tytgat, P. Dubruel, G. N. Duda, S. Van Vlierberghe and S. Geissler (2019). Extrusion printed scaffolds with varying pore size as modulators of MSC angiogenic paracrine effects. ACS Biomaterials Science & Engineering **5**(10): 5348-5358.
31. Revati, R., M. A. Majid, M. Ridzuan, M. Normahira, N. M. Nasir and A. Gibson (2017). Mechanical, thermal and morphological characterisation of 3D porous Pennisetum purpureum/PLA biocomposites scaffold. Materials Science and Engineering: C **75**: 752-759.
32. Robey, P. G. (2002). Bone matrix proteoglycans and glycoproteins. Principles of bone biology, Elsevier**:** 225-237.
33. Sadeghi, M., B. Bakhshandeh, M. M. Dehghan, M. R. Mehrnia and A. Khojasteh (2016). Functional synergy of anti-mir221 and nanohydroxyapatite scaffold in bone tissue engineering of rat skull. Journal of Materials Science: Materials in Medicine **27**(8): 132.
34. Safakhah, H. A., N. M. Kor, A. Bazargani, A. R. Bandegi, H. G. Pourbadie, B. Khoshkholgh-Sima and A. Ghanbari (2017). Forced exercise attenuates neuropathic pain in chronic constriction injury of male rat: an investigation of oxidative stress and inflammation. Journal of pain research **10**: 1457.
35. Schmitz, N., S. Laverty, V. Kraus and T. Aigner (2010). Basic methods in histopathology of joint tissues. Osteoarthritis and cartilage **18**: S113-S116.
36. Shuai, C., Y. Cheng, W. Yang, P. Feng, Y. Yang, C. He, F. Qi and S. Peng (2020). Magnetically actuated bone scaffold: Microstructure, cell response and osteogenesis. Composites Part B: Engineering **192**: 107986.

37. Szpalski, C., J. Barr, M. Wetterau, P. B. Saadeh and S. M. Warren (2010). Cranial bone defects: current and future strategies. Neurosurgical focus **29**(6): E8.
38. Talebi, A., N. H. Roodbari, H. R. Sameni and S. Zarbakhsh (2020). Impact of coadministration of apigenin and bone marrow stromal cells on damaged ovaries due to chemotherapy in rat: An experimental study. International Journal of Reproductive BioMedicine **18**(7): 551.
39. Tarafder, S., N. M. Davies, A. Bandyopadhyay and S. Bose (2013). 3D printed tricalcium phosphate scaffolds: Effect of SrO and MgO doping on in vivo osteogenesis in a rat distal femoral defect model. Biomaterials science **1**(12): 1250.
40. Tatullo, M., G. Spagnuolo, B. Codispoti, F. Zamparini, A. Zhang, M. D. Esposti, C. Aparicio, C. Rengo, M. Nuzzolese, L. Manzoli, F. Fava, C. Prati, P. Fabbri and M. G. Gandolfi (2019). PLA-based mineral-doped scaffolds seeded with human periapical cyst-derived MSCs: A promising tool for regenerative healing in dentistry. Materials **12**(4).
41. Teixeira, B. N., P. Aprile, R. H. Mendonça, D. J. Kelly and R. M. d. S. M. Thiré (2019). Evaluation of bone marrow stem cell response to PLA scaffolds manufactured by 3D printing and coated with polydopamine and type I collagen. Journal of Biomedical Materials Research Part B: Applied Biomaterials **107**(1): 37-49.
42. Tollemar, V., Z. J. Collier, M. K. Mohammed, M. J. Lee, G. A. Ameer and R. R. Reid (2016). Stem cells, growth factors and scaffolds in craniofacial regenerative medicine. Genes & diseases **3**(1): 56-71.
43. Tytgat, L., M. R. Kollert, L. Van Damme, H. Thienpont, H. Ottevaere, G. N. Duda, S. Geissler, P. Dubruel, S. Van Vlierberghe and T. H. Qazi (2020). Evaluation of 3D Printed Gelatin-Based Scaffolds with Varying Pore Size for MSC-Based Adipose Tissue Engineering. Macromolecular bioscience **20**(4): 1900364.
44. Wang, M., P. Favi, X. Cheng, N. H. Golshan, K. S. Ziemer, M. Keidar and T. J. Webster (2016). Cold atmospheric plasma (CAP) surface nanomodified 3D printed polylactic acid (PLA) scaffolds for bone regeneration. Acta biomaterialia **46**: 256-265.
45. Wang, X., C. Li and H. Gong (2017). Morphological and functional changes in bone marrow mesenchymal stem cells in rats with heart failure. Experimental and therapeutic medicine **13**(6): 2888-2892.
46. Watanabe, Y., N. Harada, K. Sato, S. Abe, K. Yamanaka and T. Matushita (2016). Stem cell therapy: is there a future for reconstruction of large bone defects? Injury **47**: S47-S51.
47. Wurm, M. C., T. Möst, B. Bergauer, D. Rietzel, F. W. Neukam, S. C. Cifuentes and C. von Wilmowsky (2017). In-vitro evaluation of Polylactic acid (PLA) manufactured by fused deposition modeling. Journal of biological engineering **11**(1): 1-9.
48. Yang, S.-l., Z.-H. Wu, W. Yang and M.-B. Yang (2008). Thermal and mechanical properties of chemical crosslinked polylactide (PLA). Polymer Testing **27**(8): 957-963.
49. Zhang, M. and N. L. Thomas (2011). Blending polylactic acid with polyhydroxybutyrate: The effect on thermal, mechanical, and biodegradation properties. Advances in Polymer Technology **30**(2): 67-79.

50. Zhang, Q., I. Nettleship, E. Schmelzer, J. Gerlach, X. Zhang, J. Wang and C. Liu (2020). Tissue engineering and regenerative medicine therapies for cell senescence in bone and cartilage. Tissue Engineering Part B: Reviews **26**(1): 64-78.
51. Zhang, Y. and M. Zhang (2004). Cell growth and function on calcium phosphate reinforced chitosan scaffolds. Journal of Materials Science: Materials in Medicine **15**(3): 255-260.
52. Zimina, A., F. Senatov, R. Choudhary, E. Kolesnikov, N. Anisimova, M. Kiselevskiy, P. Orlova, N. Strukova, M. Generalova and V. Manskikh (2020). Biocompatibility and physico-chemical properties of highly porous PLA/HA scaffolds for bone reconstruction. Polymers **12**(12): 2938.

Figures

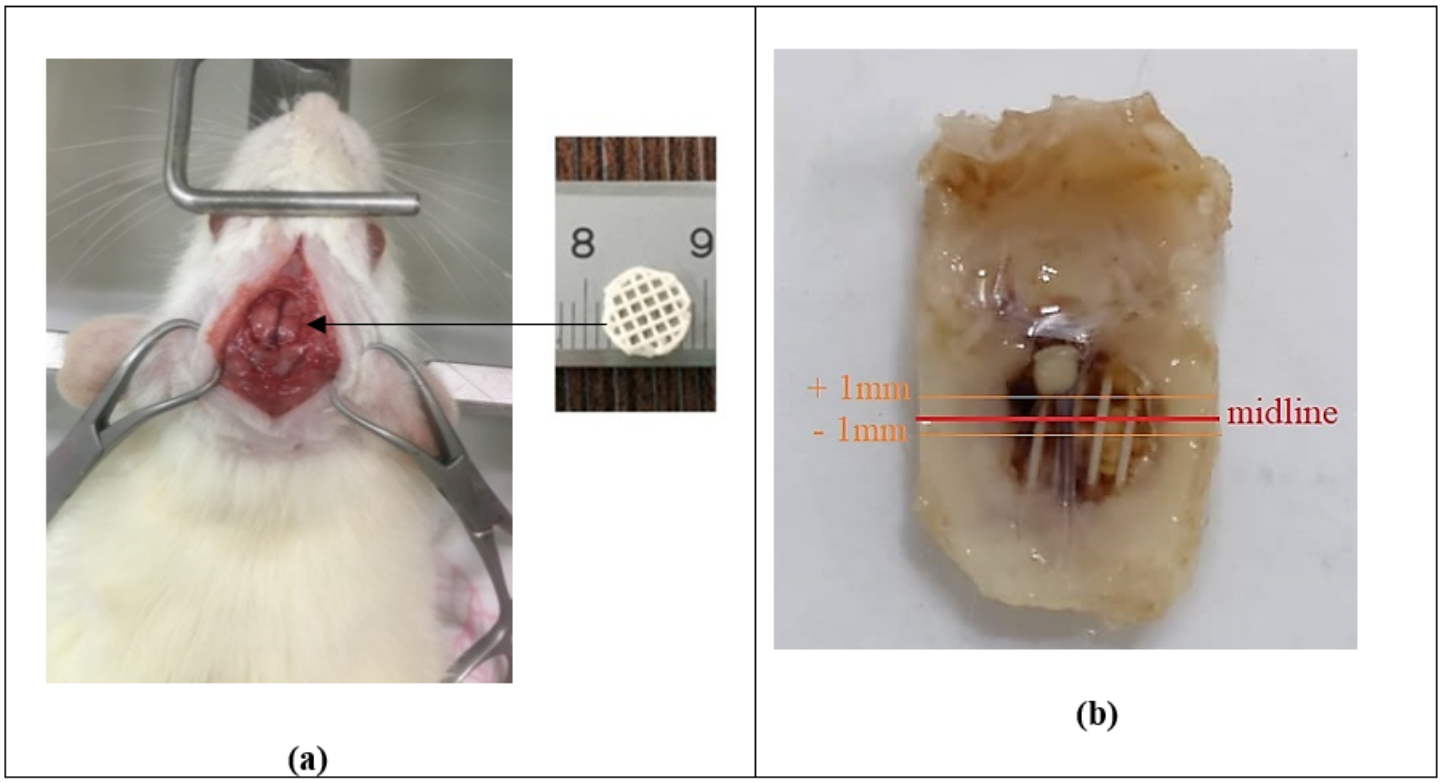

Figure 1

(a) drilled whole and 3D printed scaffold, and (b) analyzed area in histology

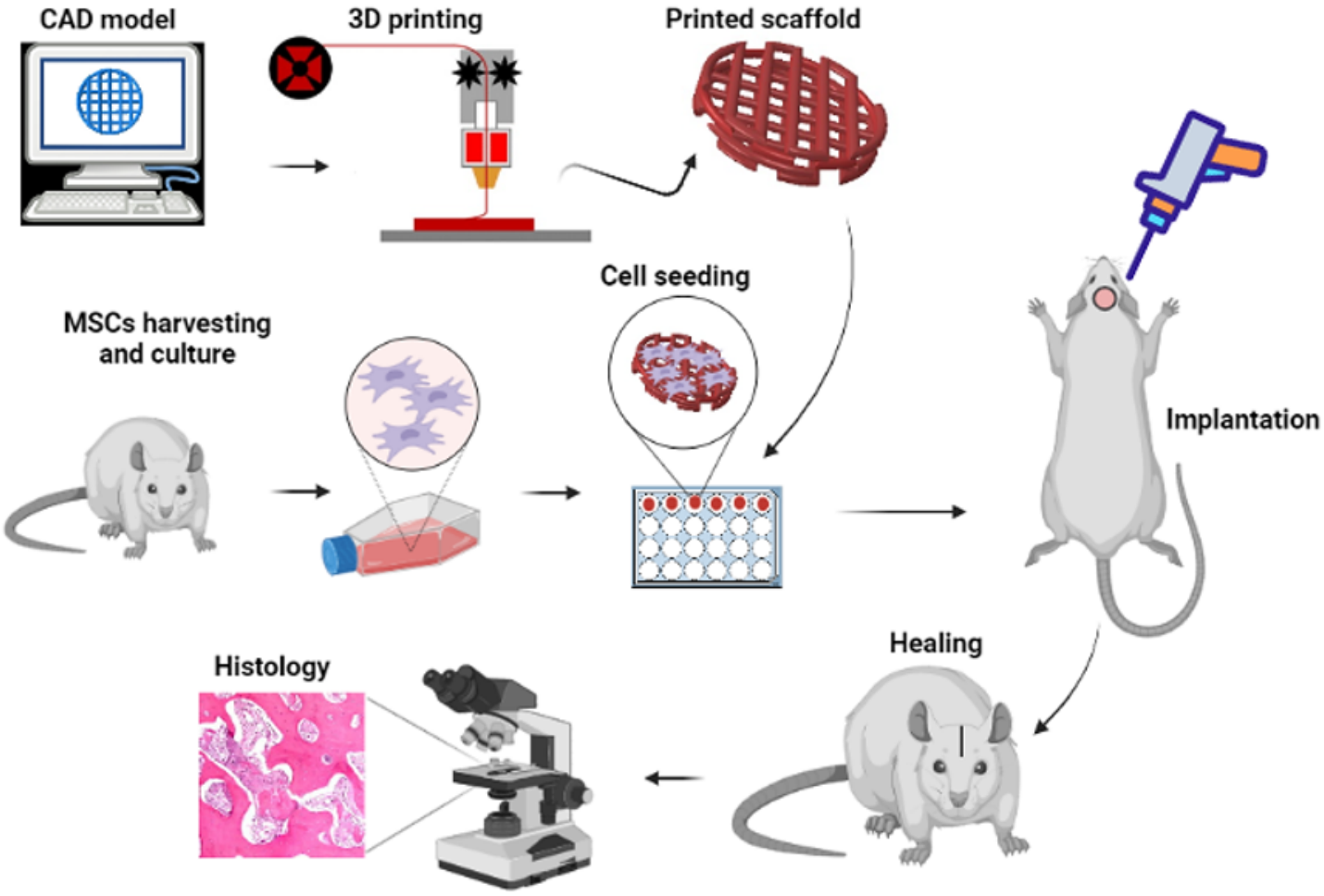

Figure 2

The general steps used in this study

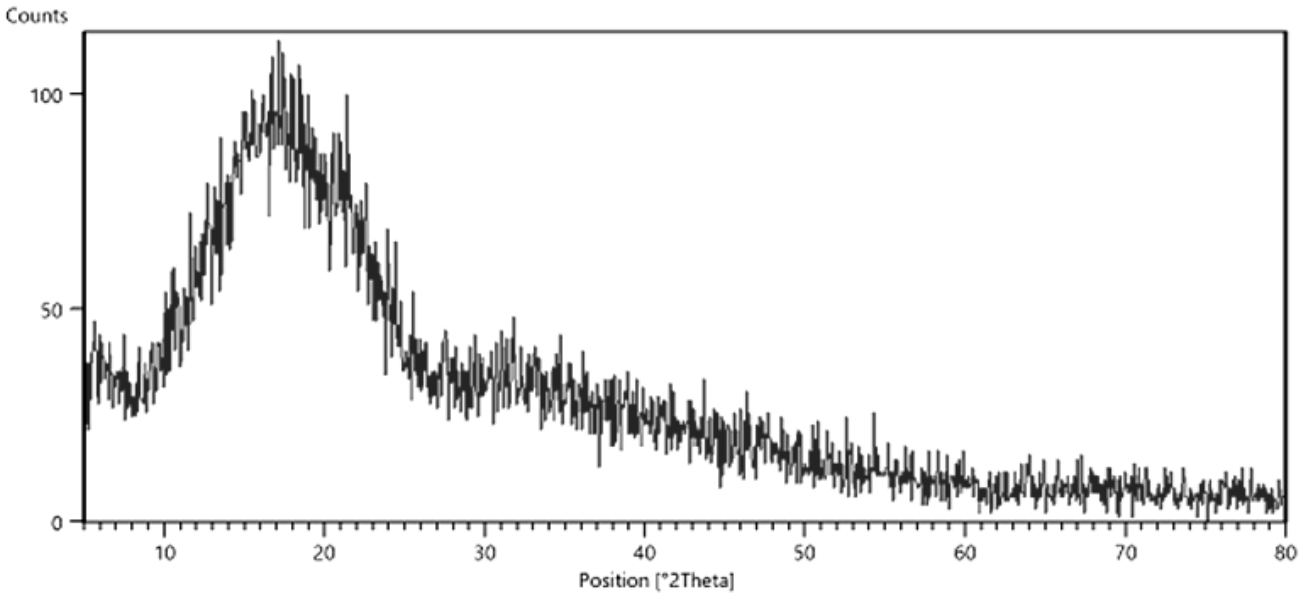

(a)

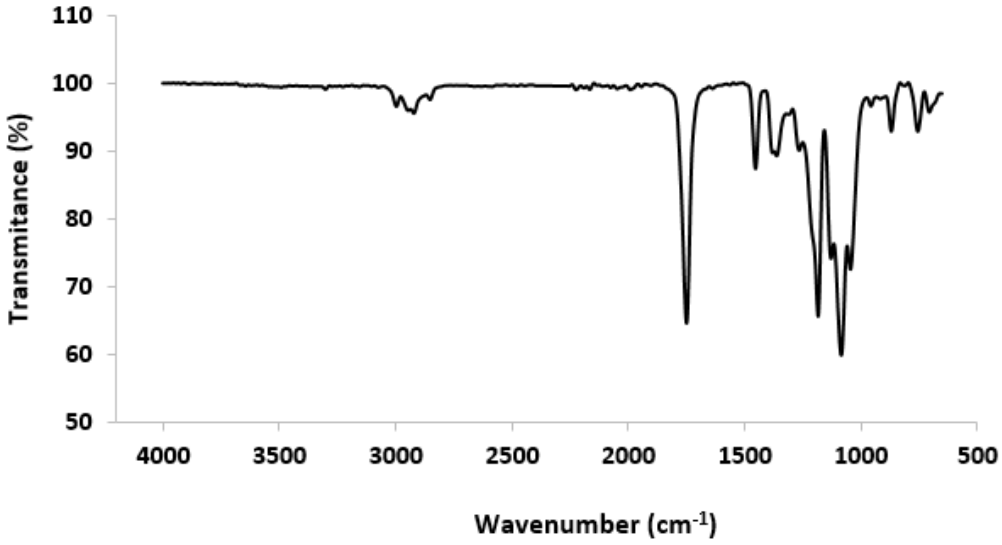

(b)

Figure 3

(a) XRD, and (b) ATR-FTIR spectra of 3D printed PLA scaffold

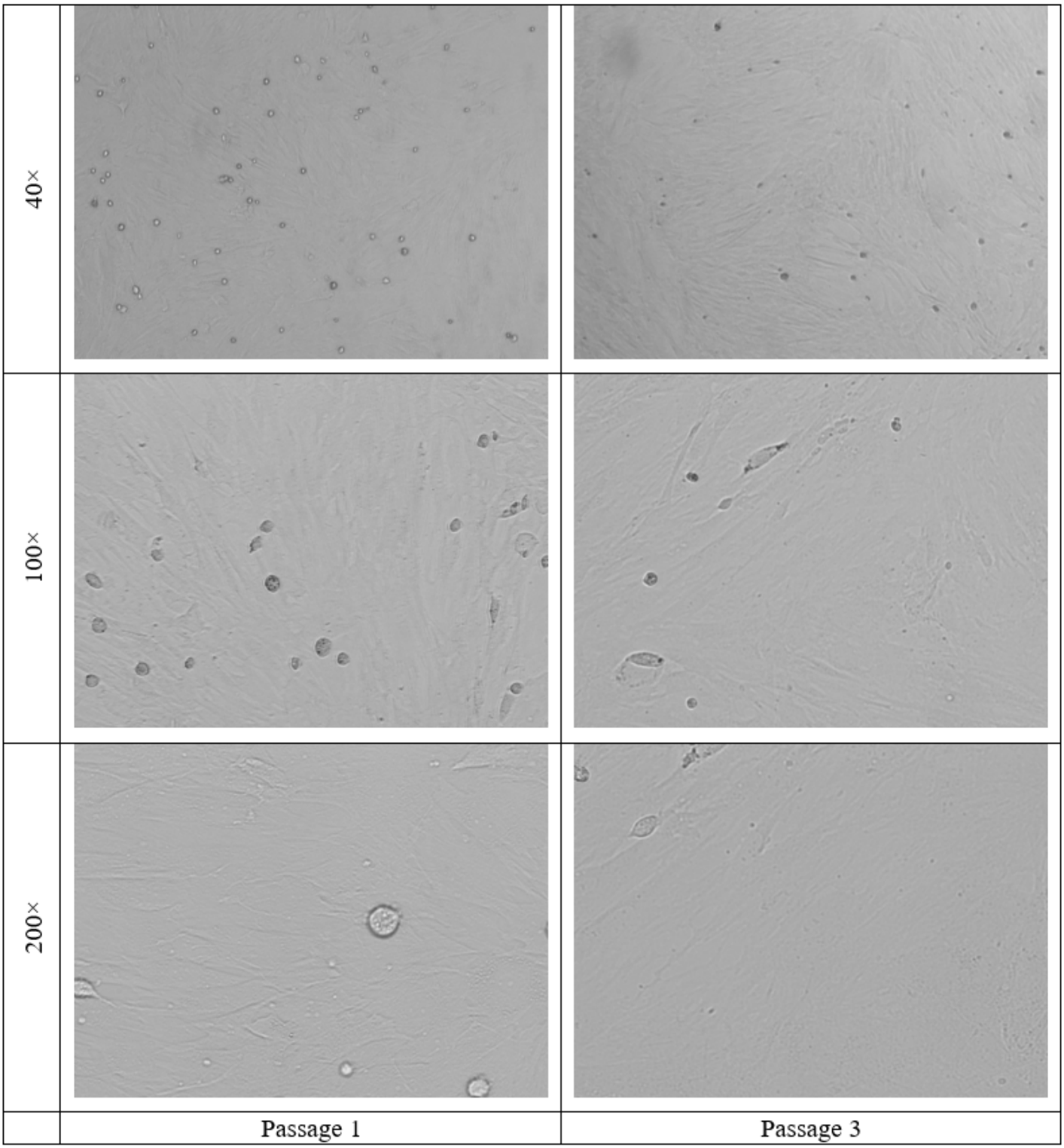

Figure 4

The morphology of BMSCs during culture

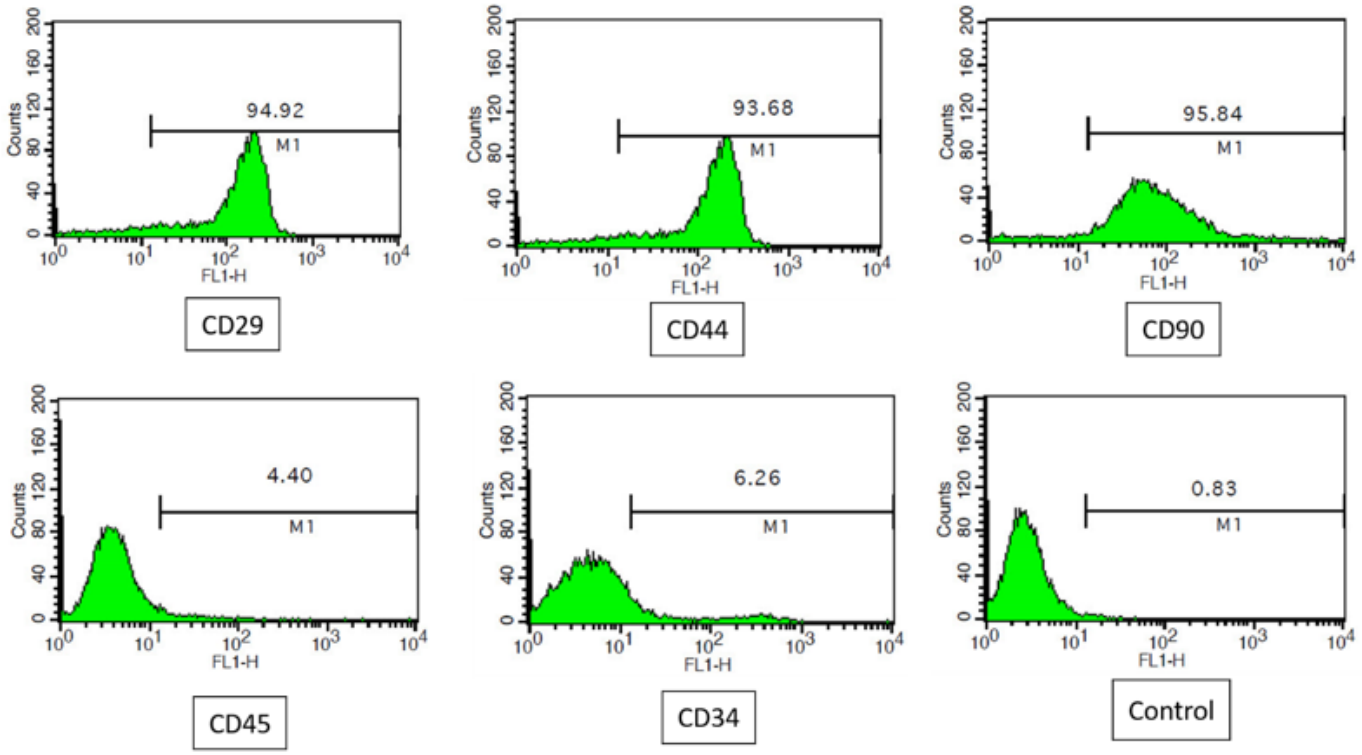

Figure 5

Flow cytometry analysis of BMSCs immunophenotype

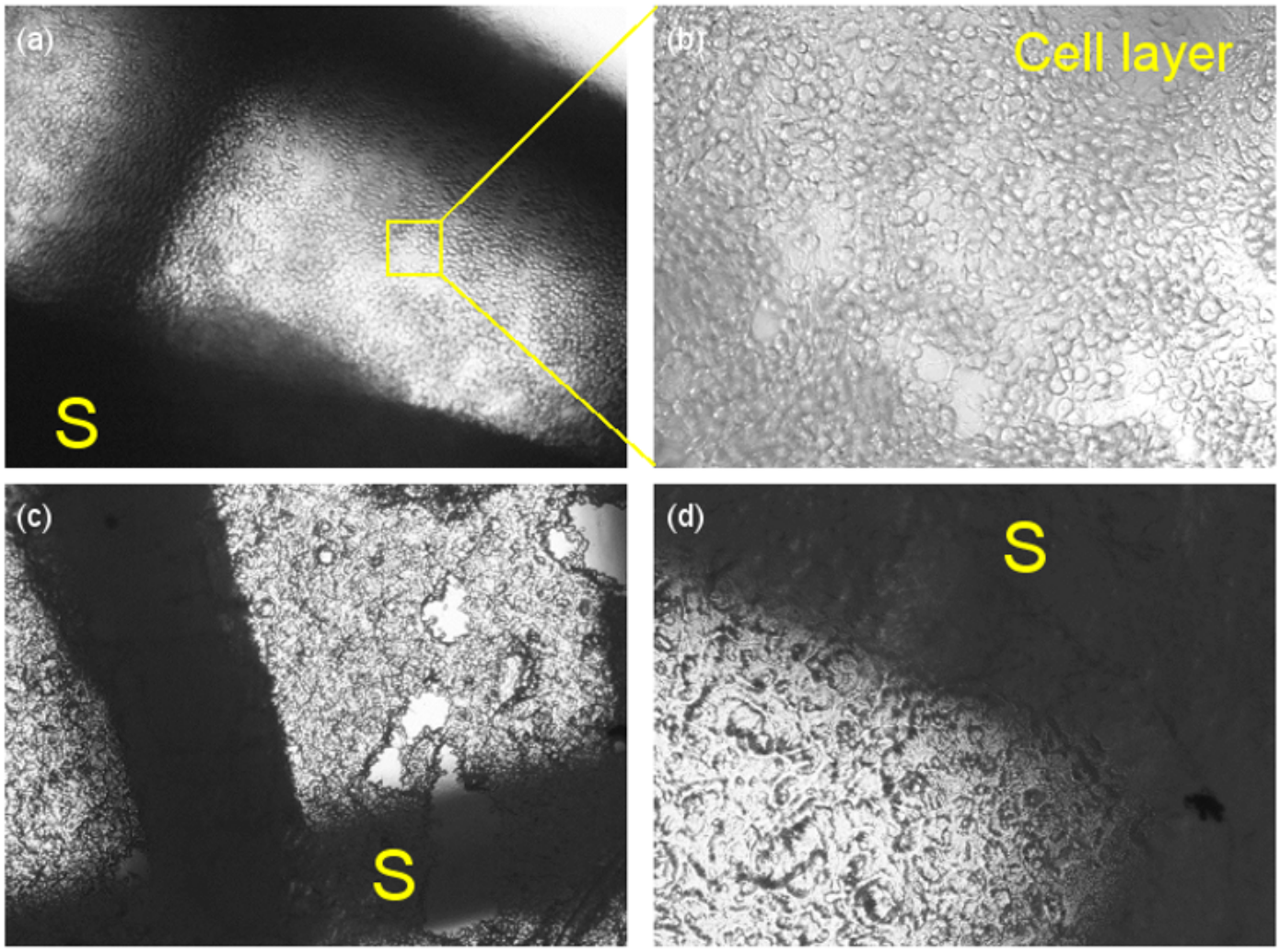

Figure 6

Cell layer on the scaffold; (a and b) live cells, and (c and d) fixed cells. The magnifications were 40× and 100× for (a and c) and (b and d), respectively. The scaffold is shown by "S".

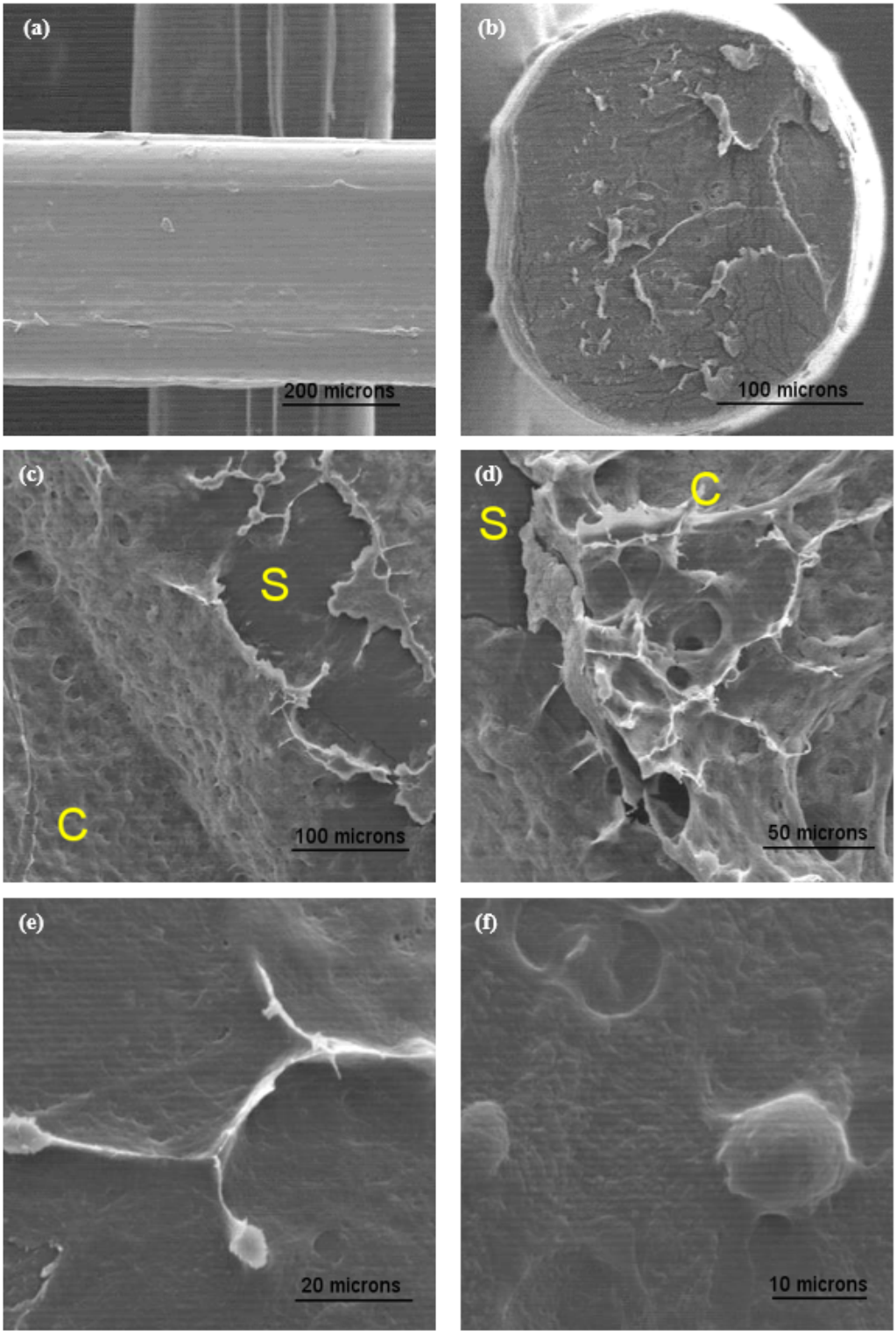

Figure 7

SEM images of (a) PLA scaffold, (b) scaffold cross-section, and (c-f) fixed cell layer on the scaffold. The scaffold and cell layer are shown by "S" and "C", respectively.

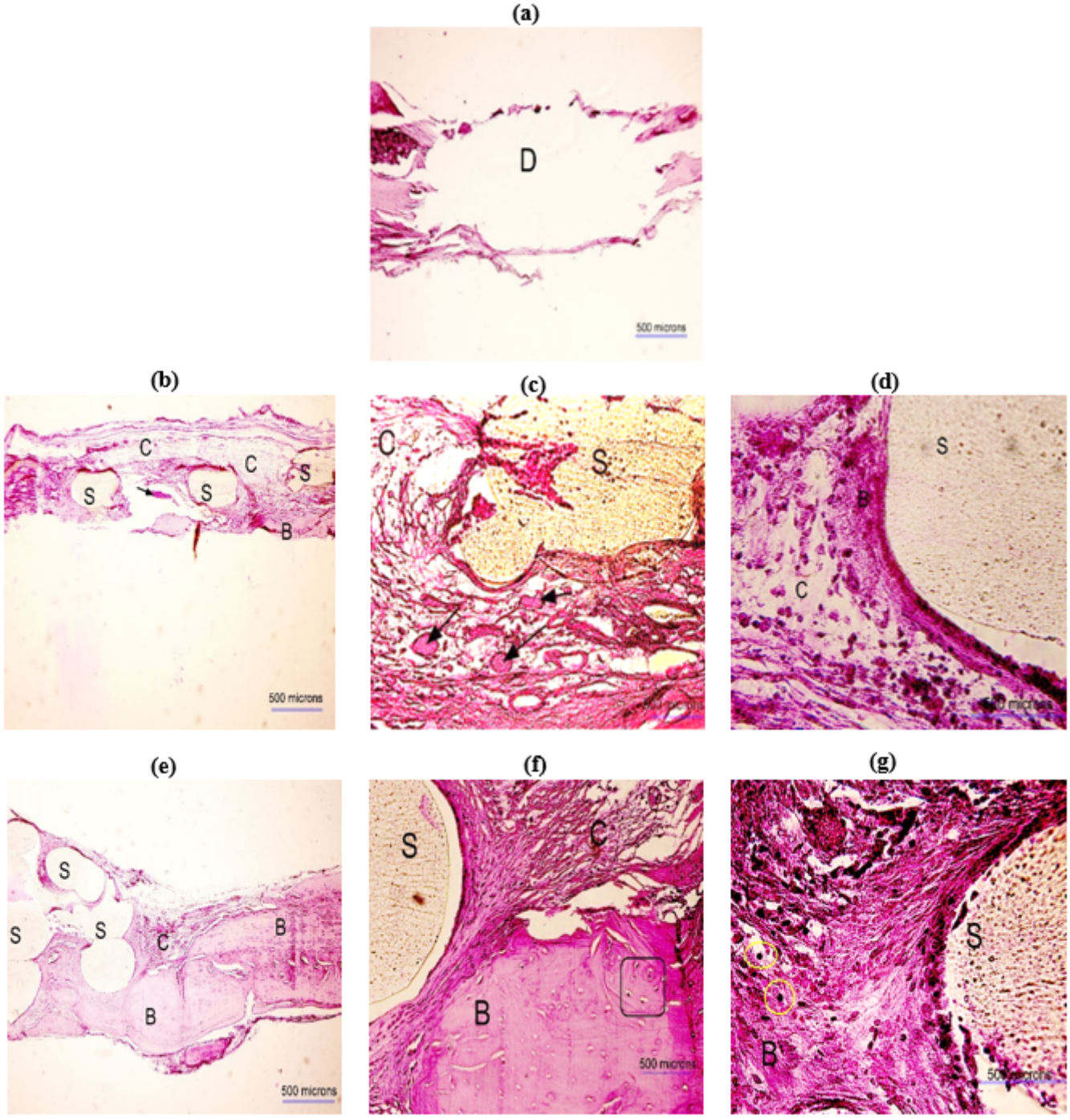

Figure 8

H&E images obtained 8 weeks postoperatively in different groups; (a) defect without scaffold, (b-d) PLA scaffold, and (e-g) PLA+Cell scaffold. The scaffold, bone, connective tissues, and defect site are shown by "S", "B", "C", and "D", respectively. The new bone islands are indicated by black arrows and osteocytes are identified in rectangles. The magnifications are ×40, ×200, and ×400 in (a, b and e), (c and f), and (d and g), respectively.

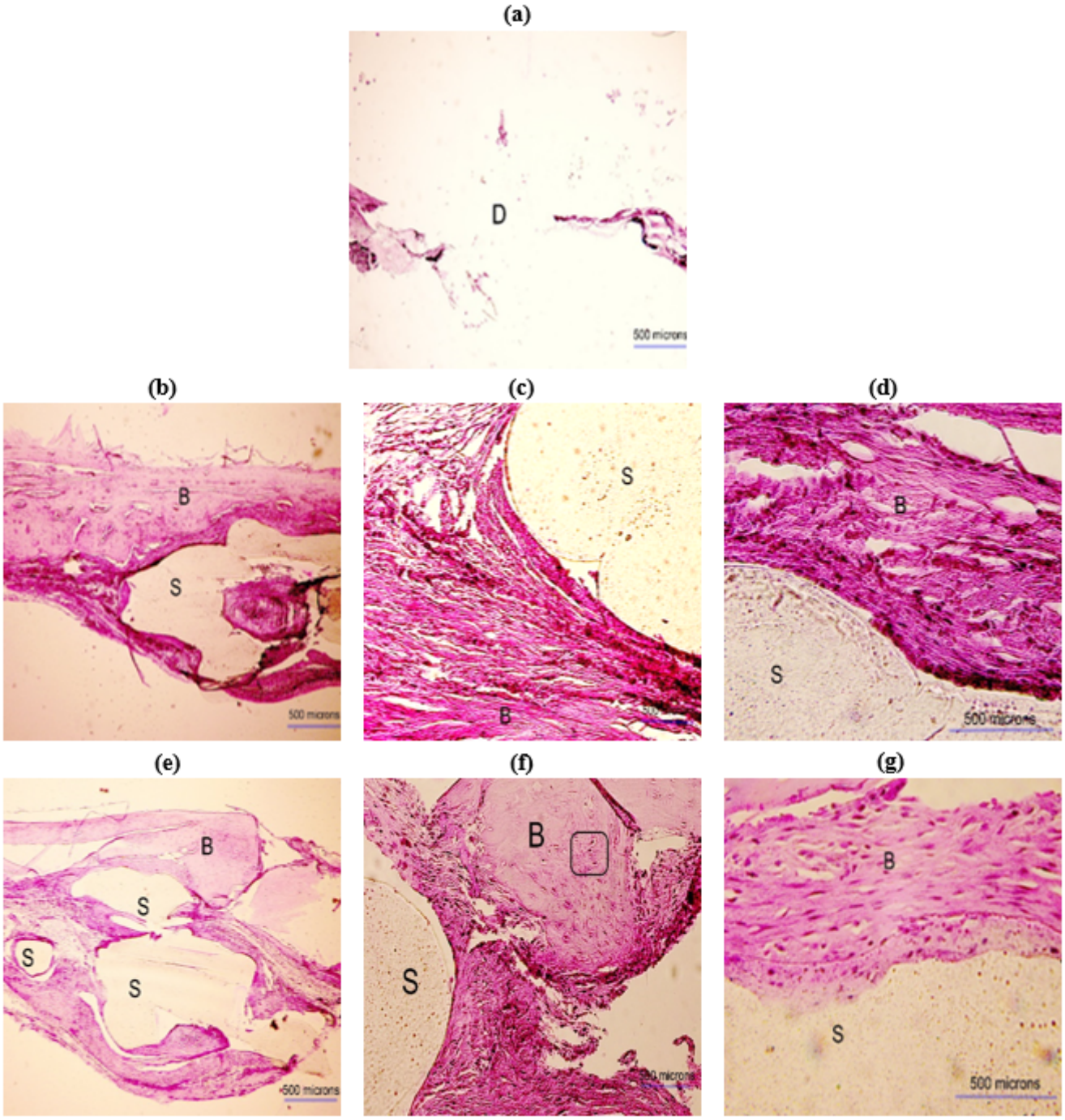

Figure 9

H&E images obtained 12 weeks postoperatively in different groups; (a) defect without scaffold, (b-d) PLA scaffold, and (e-g) PLA+Cell scaffold. The scaffold, bone, connective tissues, and defect site are shown by "S", "B", "C", and "D", respectively. The magnifications are ×40, ×200, and ×400 in (a, b and e), (c and f), and (d and g), correspondingly.

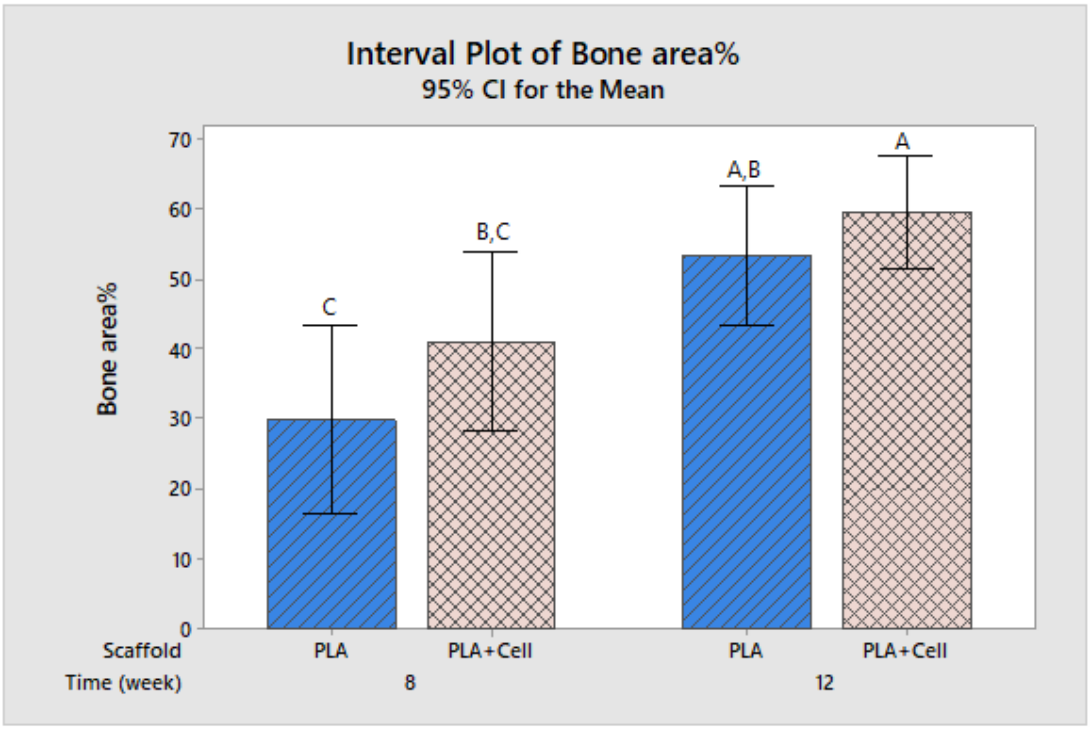

(a)

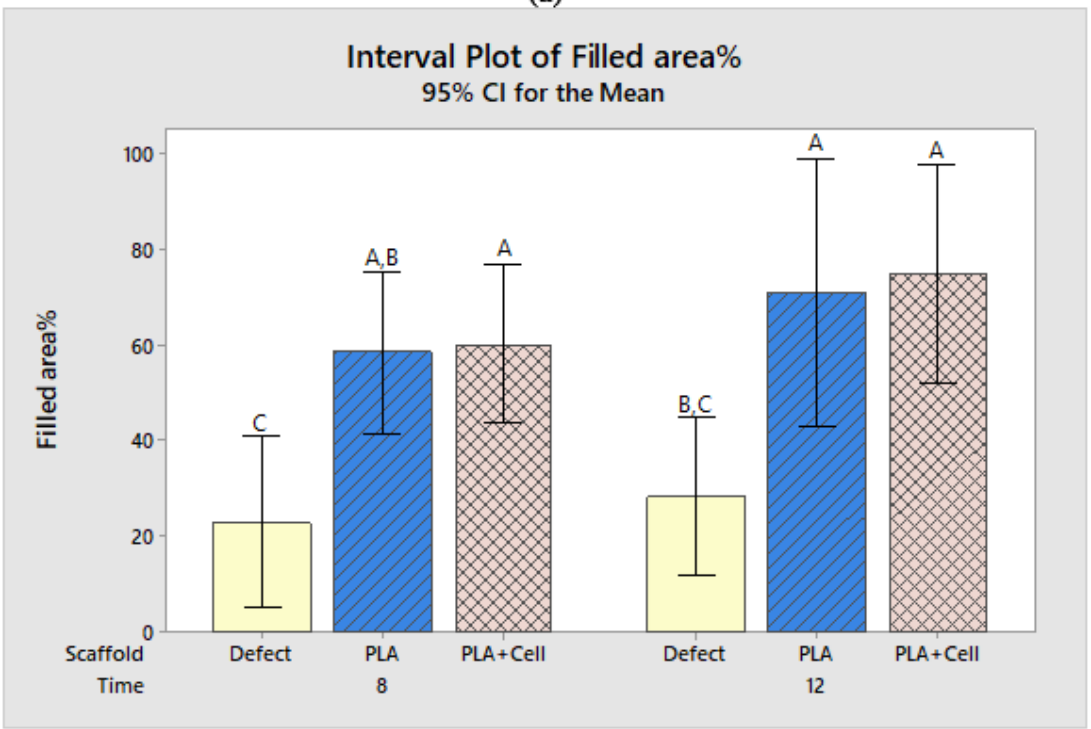

(b)

Figure 10

Comparison of (a) bone area%, and (b) filled area% in different groups (the means that do not share a letter are significantly different)

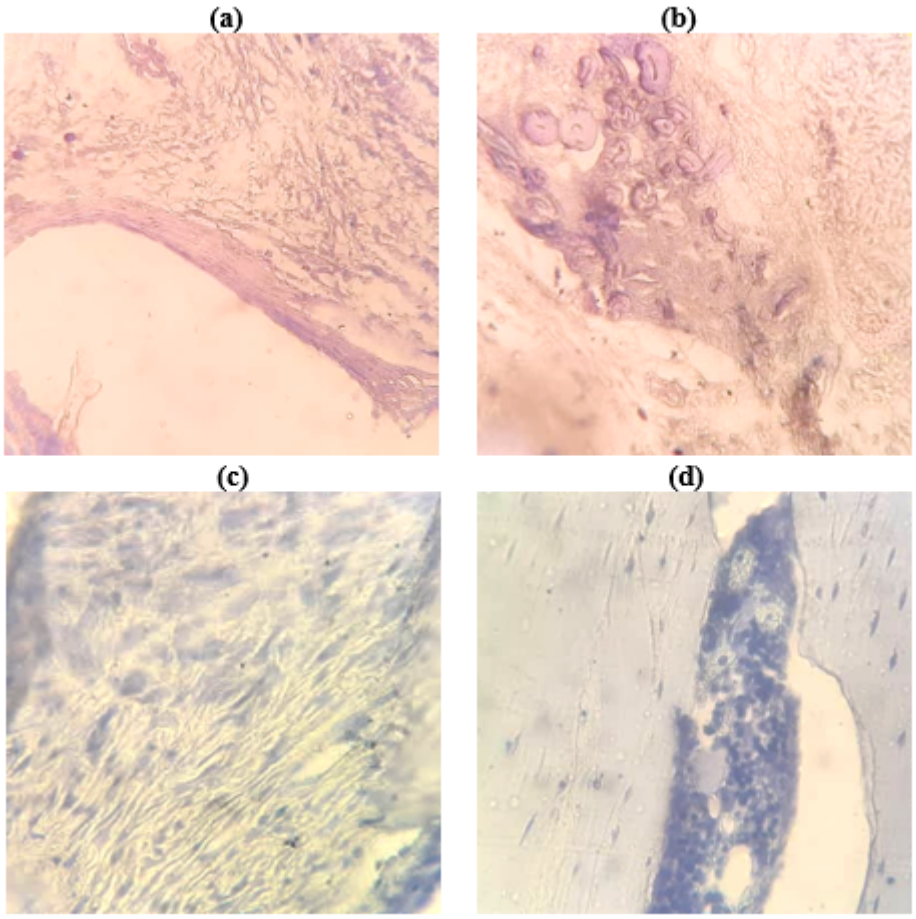

Figure 11

Toluidine blue staining obtained 8 weeks postoperatively in (a and b) PLA group, and (c and d) PLA+Cell group (×400).

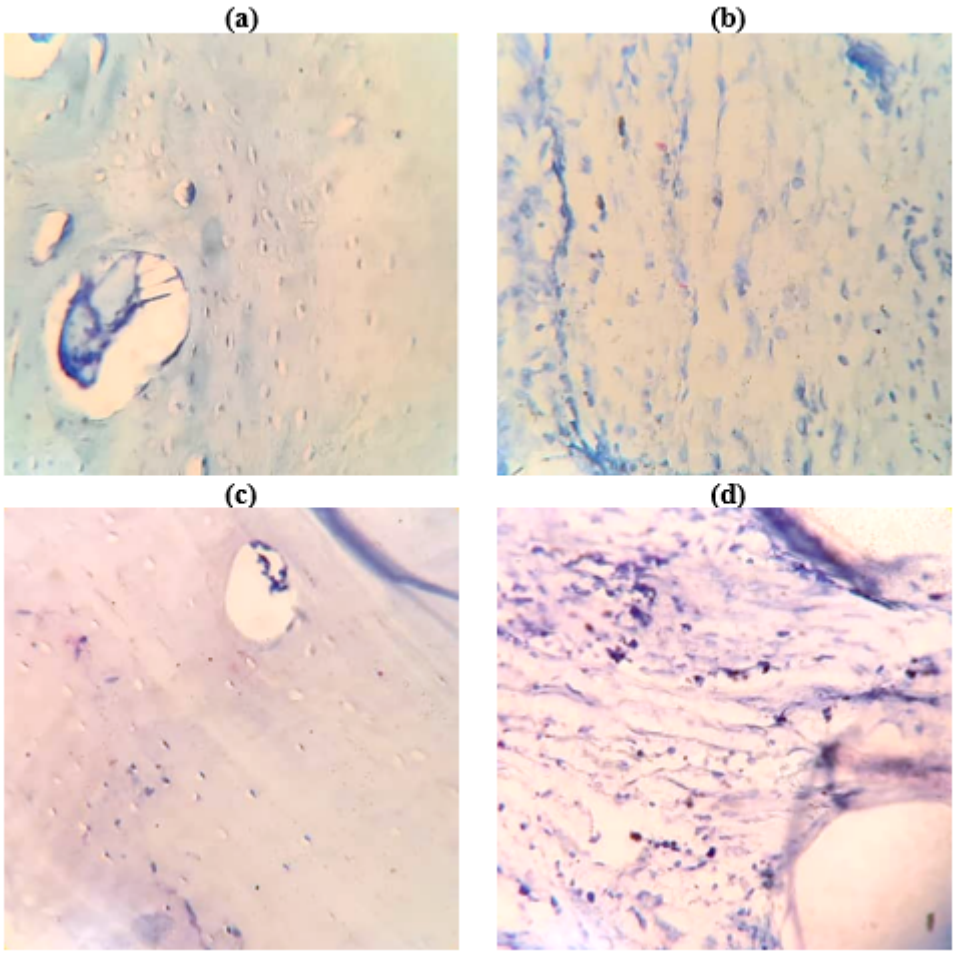

Figure 12

Toluidine blue staining obtained 12 weeks postoperatively in (a and b) PLA group, and (c and d) PLA+Cell group (×400).

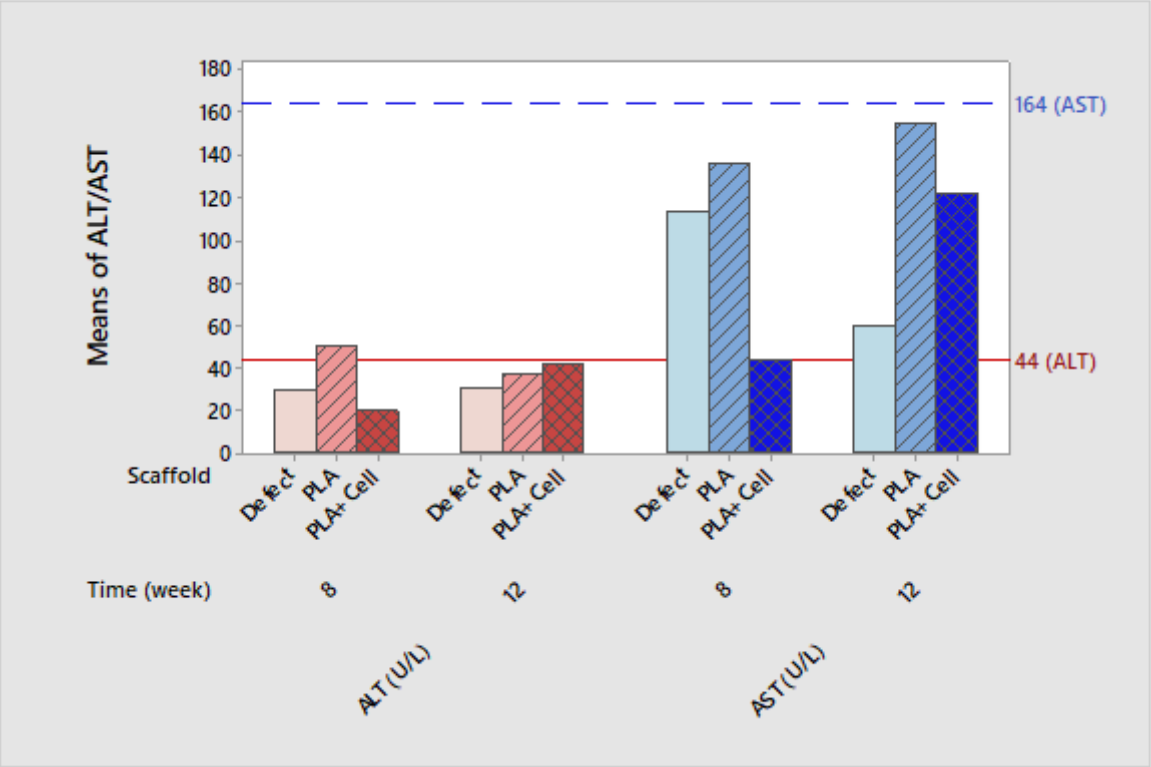

Figure 13

ALT and AST level in rat serum 8 and 12 weeks postoperatively in different groups